Linear Response Theory for Shear Modulus C_{66} and Raman Quadrupole Susceptibility: Evidence for Nematic Orbital Fluctuations in Fe-based Superconductors

Hiroshi Kontani and Youichi Yamakawa
Department of Physics, Nagoya University, Furo-cho, Nagoya 464-8602, Japan
(Received 8 December 2013; published 25 July 2014)

The emergence of the nematic order and fluctuations has been discussed as a central issue in Fe-based superconductors. To clarify the origin of the nematicity, we focus on the shear modulus C_{66} and the Raman quadrupole susceptibility $\chi^{\rm Raman}_{x^2-y^2}$. Because of the Aslamazov-Larkin vertex correction, the nematic-type orbital fluctuations are induced, and they enhance both $1/C_{66}$ and $\chi^{\rm Raman}_{x^2-y^2}$ strongly. However, $\chi^{\rm Raman}_{x^2-y^2}$ remains finite even at the structure transition temperature T_S, because of the absence of the band Jahn-Teller effect and the Pauli (intraband) contribution, as proved in terms of the linear response theory. The present study clarifies that the origin of the nematicity in Fe-based superconductors is the nematic orbital order and fluctuations.

DOI: 10.1103/PhysRevLett.113.047001 PACS numbers: 74.70.Xa, 74.25.Ld, 74.25.nd, 74.40.Kb

In Fe-based superconductors, the nematic order and fluctuations attract great attention as one of the essential properties of the electronic states. A schematic phase diagram of $BaFe_2As_2$ as a function of carrier doping y is shown in Fig. 1: For $y > 0$ (electron doping), the nonmagnetic orthorhombic (C_2) phase transition occurs at T_S, and the antiferromagnetic spin order is realized at T_N ($\lesssim T_S$) in the C_2 phase. In $Ba(Fe_{1-x}Co_x)_2As_2$ ($y = x$), both the structural and magnetic quantum critical points (QCPs) are very close, and strong magnetic fluctuations are observed near the QCPs by nuclear magnetic resonance (NMR) [1]. In addition, strong nematic susceptibility that couples to the C_2 structure deformation had been observed via the softening of shear modulus C_{66} [2–6] and in-plane anisotropy of resistivity [7]. Similar softening of C_{66} is also observed in $(Ba_{1-x}K_x)Fe_2As_2$ ($y = -x/2$; hole doping) [5] and Fe(Se,Te) ($y = 0$) [8]. Interestingly, in $Ba(Fe_{1-x}Ni_x)_2As_2$ ($y = 2x$), magnetic QCP and structural QCP are well separated, and quantum ciriticalities are realized at both points [9].

Then, a natural question is, what is the "nematic order parameter" that would be closely related to the pairing mechanism? Up to now, both the spin-nematic mechanism [2] and ferro-orbital order mechanism [10–13] had been proposed, and the softening of C_{66} can be fitted by both mechanisms [14,15]. The former predicts that the spin-nematic order $\langle \boldsymbol{s}_i \cdot \boldsymbol{s}_{i+\hat{x}} \rangle \neq 0$ occurs above T_N when the magnetic order $\langle \boldsymbol{s}_i \rangle$ is suppressed by the J_1-J_2 frustration. As for the latter scenario, it was shown that the nematic orbital order $n_{xz} \neq n_{yz}$ is induced by spin fluctuations, due to strong spin-orbital mode coupling given by the vertex correction (VC) [13,16,17]. The large d-orbital level splitting $E_{yz} - E_{xz} \sim 60$ meV in the C_2 phase [18,19] may be too large to be produced by spin-nematic order via spin-lattice coupling.

Recently observed large quadrupole susceptibility $\chi^{\rm Raman}_{x^2-y^2}$ by electron Raman spectroscopy [20,21] presents a direct evidence of the strong orbital fluctuations. Although this result favors the orbital-nematic scenario, the observed enhancement of $\chi^{\rm Raman}_{x^2-y^2}$ is apparently smaller than the orbital susceptibility extracted from C_{66}. For example, $\chi^{\rm Raman}_{x^2-y^2}$ remains finite at $T = T_S$, although C^{-1}_{66} diverges at T_S. Therefore, it should be verified whether or not both C_{66} and $\chi^{\rm Raman}_{x^2-y^2}$ can be explained based on the orbital-nematic scenario.

In this Letter, we analyze both C_{66} and $\chi^{\rm Raman}_{x^2-y^2}$, both of which are key experiments to uncover the nematic order parameter. It is found that both C_{66} and $\chi^{\rm Raman}_{x^2-y^2}$ are enhanced

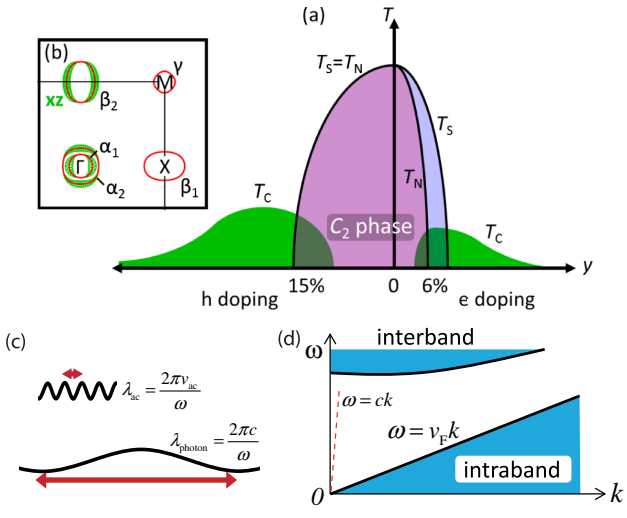

FIG. 1 (color online). (a) Schematic phase diagram of Fe-based superconductors. (b) Fermi surfaces for $y = 0$. The weight of the d_{xz} orbital is stressed by green circles. (c) Relation $\lambda_{\rm photon} \gg \lambda_{\rm ac}$. (d) Particle-hole excitation continuum.

by the orbital fluctuations due to Aslamazov-Larkin-type (AL) VC. However, $\chi^{\rm Raman}_{x^2-y^2}$ is less singular since the band Jahn-Teller (JT) effect and the Pauli (intraband) quadrupole susceptibilities do not contribute to $\chi^{\rm Raman}_{x^2-y^2}$. Since both C_{66} and $\chi^{\rm Raman}_{x^2-y^2}$ are explained satisfactorily, the orbital-nematic scenario is essential for many Fe-based superconductors.

As for the pairing mechanism, at present, both the spin-fluctuation-mediated $s_{\pm}$-wave state [22–24] and the orbital-fluctuation-mediated s_{++}-wave state [25,26] have been discussed. When both fluctuations coexist, the nodal s-wave state can be realized [27]. The s_{++}-wave state is consistent with the robustness of T_c against impurities [28,29] and the broad hump structure in the inelastic neutron scattering [30,31]. The self-consistent VC method [13,26] predicts the developments of ferro- and antiferro-orbital fluctuations, and the freezing of the latter fluctuations would explain the nematic order at $T^* \sim 200$ K ($\gg T_S$) [32,33].

First, we discuss the susceptibility at $\boldsymbol{k} \approx \boldsymbol{0}$ with respect to the quadrupole order parameter $\hat{O}_{x^2-y^2} \equiv n_{xz} - n_{yz}$ in the Hubbard model. For $U = U' + 2J$, it is approximately given as [13,16]

$$\chi_{x^2-y^2}(k) = 2\Phi(k)/[1 - (U - 5J)\Phi(k)], \tag{1}$$

where $k = (\boldsymbol{k}, \omega)$, and $\Phi(k) \equiv \chi^{(0)}(k) + X(k)$ is the intra-orbital (within d_{xz} orbital) irreducible susceptibility: $\chi^{(0)}(k)$ is the noninteracting susceptibility and $X(k)$ is the VC for the charge channel. The nematic orbital order $n_{xz} \neq n_{yz}$ occurs when the charge Stoner factor $\alpha_c = (U - 5J)\Phi(0)$ reaches unity, which is realized near the magnetic QCP since the AL-VC is proportional to the square of the magnetic correlation length [13,16,17].

Next, we discuss the "total" quadrupole susceptibility in real systems, by including the realistic quadrupole interaction due to the acoustic phonon for the ortho-rhombic distortion. According to Ref. [34], it is given as $-g_{\rm ac}(k)\hat{O}_{x^2-y^2}(\boldsymbol{k})\hat{O}_{x^2-y^2}(-\boldsymbol{k})$, where $\hat{O}_{x^2-y^2}(\boldsymbol{k})$ is the quadrupole operator, and $g_{\rm ac}(k) = g(v_{\rm ac}|\boldsymbol{k}/\omega|)^2/[(v_{\rm ac}|\boldsymbol{k}/\omega|)^2 - 1]$ is the phonon propagator multiplied by the coupling constants. $v_{\rm ac}$ is the phonon velocity. Since the Migdal's theorem tells us that the effect of g on the irreducible susceptibility is negligible, the total susceptibility is

$$\chi^{\rm tot}_{x^2-y^2}(k) = \chi_{x^2-y^2}(k)/[1 - g_{\rm ac}(k)\chi_{x^2-y^2}(k)]. \tag{2}$$

Now, we discuss the acoustic and optical responses based on the total susceptibility (2), by noting that any susceptibilities in metals are *discontinuous* at $\omega = |\boldsymbol{k}| = 0$. Since the elastic constant is measured under the static ($\omega = 0$) strain with long wavelength ($|\boldsymbol{k}| \to 0$), C_{66} is given as

$$C_{66}^{-1} \sim 1 + \lim_{\boldsymbol{k}\to\boldsymbol{0}} g_{\rm ac}(\boldsymbol{k}, 0)\chi^{\rm tot}_{x^2-y^2}(\boldsymbol{k}, 0) = \frac{1}{1 - g\chi_{k\text{-lim}}}, \tag{3}$$

where $\chi_{k\text{-lim}} \equiv \lim_{\boldsymbol{k}\to\boldsymbol{0}}\chi_{x^2-y^2}(\boldsymbol{k}, 0)$ is called the k-limit, and the relation $g_{\rm ac}(k) = g$ for $\omega = 0$ is taken into account. The structure transition occurs when C_{66}^{-1} diverges. When the AL-VC is negligible, $\chi_{k\text{-lim}}$ is as small as $\chi^{(0)}_{k\text{-lim}}$. Even in this case, C_{66}^{-1} can diverge when g is very large, which is known as the band JT effect. However, the band JT mechanism cannot explain the strong enhancement of $\chi^{\rm Raman}_{x^2-y^2}$, as we will clarify later. In fact, the fitting of experimental data in this Letter indicates that the softening of C_{66} is mainly given by the AL-VC: The relation $1/g \sim \chi_{k\text{-lim}} \gg \chi^{(0)}_{k\text{-lim}}$ is satisfied in Fe-based superconductors.

Next, we derive the optical response in the dc limit, measured by using the low-energy photon with $k = (\boldsymbol{k}, \omega = c|\boldsymbol{k}|)$ and $\omega \to 0$. Considering that the photon velocity c is much faster than the Fermi velocity v_F and $v_{\rm ac}$, it is given as

$$\chi^{\rm Raman}_{x^2-y^2} \sim \lim_{\omega\to 0}\chi^{\rm tot}_{x^2-y^2}(\boldsymbol{0}, \omega) = \chi_{\omega\text{-lim}}, \tag{4}$$

where $\chi_{\omega\text{-lim}} \equiv \lim_{\omega\to 0}\chi_{x^2-y^2}(\boldsymbol{0}, \omega)$ is called the ω-limit [35,36]. Since $g_{\rm ac}(k)$ is zero for $|\omega/\boldsymbol{k}| = c$, the band JT effect does not contribute to the Raman susceptibility. The physical explanation is that the acoustic phonons cannot be excited by photons because of the mismatch of the wavelengths $\lambda_{\rm photon} \gg \lambda_{\rm ac}$ for the same ω as shown in Fig. 1(c). Also, since $c \gg v_F$, low-energy photon cannot induce the intraband particle-hole excitation as understood from the location of the particle-hole continuum shown in Fig. 1(d). This fact leads to the relationship "$\chi_{\omega\text{-lim}}$ is smaller than $\chi_{k\text{-lim}}$," as we discuss mathematically later. For the charge quadrupole susceptibility, this relationship holds even if the quasiparticle lifetime is finite due to impurity scattering; see the Supplemental Material [37]. Therefore, $\chi^{\rm Raman}_{x^2-y^2}$ remains finite at $T \sim T_S$ although C_{66}^{-1} diverges at T_S, consistently with experiments [20,21].

Hereafter, we perform the numerical calculation of the quadrupole susceptibility in the five-orbital model. The unit of energy is eV unless otherwise noted. First, we discuss the k-limit and ω-limit of the bare bubble made of two d_{xz} orbital Green functions. They are connected by the following relation:

$$\chi^{(0)}_{k\text{-lim}} = \chi^{(0)}_{\omega\text{-lim}} + \sum_{\alpha}^{\rm band}\sum_{\boldsymbol{k}}\left(-\frac{\partial f^{\alpha}_{\boldsymbol{k}}}{\partial \epsilon^{\alpha}_{\boldsymbol{k}}}\right)\{z^{\alpha}_{\boldsymbol{k}}\}^2, \tag{5}$$

where $z^{\alpha}_{\boldsymbol{k}} = |\langle xz, \boldsymbol{k}|\alpha, \boldsymbol{k}\rangle|^2 \le 1$ is the weight of the d_{xz} orbital on band α, and $f^{\alpha}_{\boldsymbol{k}} = \{\exp[(\epsilon^{\alpha}_{\boldsymbol{k}} - \mu)/T] + 1\}^{-1}$. In Eq. (5), $\chi^{(0)}_{\omega\text{-lim}} = \sum^{\rm band}_{\alpha\neq\beta}\sum_{\boldsymbol{k}}(f^{\alpha}_{\boldsymbol{k}} - f^{\beta}_{\boldsymbol{k}})/(\epsilon^{\beta}_{\boldsymbol{k}} - \epsilon^{\alpha}_{\boldsymbol{k}})z^{\alpha}_{\boldsymbol{k}}z^{\beta}_{\boldsymbol{k}}$ is given by only the interband ($\alpha \neq \beta$) contribution, which is called the Van Vleck term. Therefore, $\chi^{(0)}_{k\text{-lim}}$ is always

larger than $\chi^{(0)}_{\omega\text{-lim}}$ due to the intraband contribution given by the second term in Eq. (5), called the Pauli term. We obtain $\chi^{(0)}_{\omega\text{-lim}} \approx 0.25$ and $\chi^{(0)}_{k\text{-lim}} \approx 0.45$ in the present model.

Next, we analyze AL-VC in detail, since it is the main driving force of the orbital fluctuations. The analytic expression of the AL term is given in Refs. [13,16]. To simplify the discussion, we consider the intraorbital (within d_{xz} orbital) AL term. Then, $X_{k(\omega)\text{-lim}}$ is approximately given as

$$X_{k(\omega)\text{-lim}} = 3T\sum_{\boldsymbol{q}} |\Lambda^{k(\omega)\text{-lim}}_{\boldsymbol{q}}|^2 V^s(\boldsymbol{q},0)^2, \tag{6}$$

where $\Lambda^{\omega\text{-lim}}_{\boldsymbol{q}} \equiv \lim_{\omega\to 0}\Lambda_q(\boldsymbol{0},\omega)$ and $\Lambda^{k\text{-lim}}_{\boldsymbol{q}} \equiv \lim_{\boldsymbol{k}\to\boldsymbol{0}}\Lambda_q(\boldsymbol{k},0)$ at $q=(\boldsymbol{q},0)$: $\Lambda_{\boldsymbol{q}}(\boldsymbol{k},0)$ is the three-point vertex made of three Green functions [13]. Also, $V^s(q) = U + U^2\chi^s(q)$, where $\chi^s(q)$ is the spin susceptibility for the d_{xz} orbital. Here, we assume the following Millis-Monien-Pines form of $\chi^s(q)$ [38]:

$$\chi^s(q) = c\xi^2[1 + \xi^2(\boldsymbol{q}-\boldsymbol{Q})^2 + |\Omega_m|/\omega_{\text{sf}}]^{-1}, \tag{7}$$

where $\boldsymbol{Q} = (0,\pm\pi)$, $\xi^2 = l/(T-\theta)$ is the square of the spin correlation length, and $\omega_{\text{sf}} = l'\xi^{-2}$ is the spin-fluctuation energy scale. Quantitatively speaking, $X_{k(\omega)\text{-lim}}$ given by Eq. (6) is underestimated since nonzero Matsubara terms are dropped. However, in the classical region $\omega_{\text{sf}} < 2\pi T$, which is realized in optimally doped $Ba(Fe,Co)_2As_2$ [39], $\chi^s(\boldsymbol{q},\omega_l)$ for $l \neq 0$ is negligibly small. In this case, we can safely use Eq. (6).

According to Eqs. (6) and (7), we obtain $X_{k(\omega)\text{-lim}} \sim T\{\Lambda^{k(\omega)\text{-lim}}_{\boldsymbol{Q}}\}^2\xi^2$ for two-dimensional systems. $\Lambda^{k\text{-lim}}_{\boldsymbol{q}}$ and $\Lambda^{\omega\text{-lim}}_{\boldsymbol{q}}$ are connected by the following relation:

$$\Lambda^{k\text{-lim}}_{\boldsymbol{q}} = \Lambda^{\omega\text{-lim}}_{\boldsymbol{q}} + \sum_{\alpha,\gamma}\sum_{\boldsymbol{k}}\left(-\frac{\partial f^{\alpha}_{\boldsymbol{k}}}{\partial\epsilon^{\alpha}_{\boldsymbol{k}}}\right)\frac{\{z^{\alpha}_{\boldsymbol{k}}\}^2 z^{\gamma}_{\boldsymbol{k}-\boldsymbol{q}}}{\epsilon^{\gamma}_{\boldsymbol{k}-\boldsymbol{q}} - \epsilon^{\alpha}_{\boldsymbol{k}}}, \tag{8}$$

where $\Lambda^{\omega\text{-lim}}_{\boldsymbol{q}}$ is the interband Van Vleck term [40]. For $\boldsymbol{q}\approx\boldsymbol{Q}$, $\Lambda^{k\text{-lim}}_{\boldsymbol{q}}$ increases strongly at low T, because of the intraband Pauli term in the second term of Eq. (8). Its main contribution is given by $\alpha = \alpha_{1,2}$ and $\gamma = \beta_2$ in Fig. 1(b). Both the Pauli and Van Vleck terms are negative in the present model. Therefore, the relationship $X_{k\text{-lim}} > X_{\omega\text{-lim}}$ is satisfied.

Figure 2(a) shows the temperature dependence of $X_{k\text{-lim}}/T$ given by Eq. (6), by using the static RPA spin susceptibility $\chi^s(\boldsymbol{q},0)$ obtained at $T=0.01$. In this calculation, $\xi^2 \propto (1-\alpha_s)^{-1}$ is fixed, where $\alpha_s = U\chi^{(0)}(\boldsymbol{Q},0)$ is the spin Stoner factor. Thus, we obtain the relationship $X_{k\text{-lim}}/T \sim T^{-0.5}\xi^2$, in which the factor $T^{-0.5}$ originates from the strong T dependence of $|\Lambda^{k\text{-lim}}_{\boldsymbol{Q}}|^2$. We also show the temperature dependence of $X_{\omega\text{-lim}}/T$ in Fig. 2(b): The

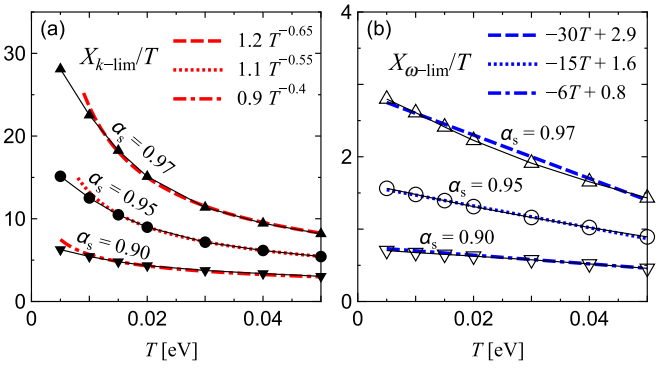

FIG. 2 (color online). (a) $X_{k\text{-lim}}/T$ and (b) $X_{\omega\text{-lim}}/T$ as functions of T. Their T dependences originate from $|\Lambda^{k(\omega)\text{-lim}}_{\boldsymbol{Q}}|^2$ since $\xi^2 \propto 1/(1-\alpha_s)$ is fixed.

relation $X_{\omega\text{-lim}}/T \sim (b-T)\xi^2$ is realized due to the T dependence of $|\Lambda^{\omega\text{-lim}}_{\boldsymbol{Q}}|^2$ [40]. Therefore, the relationship $X_{k\text{-lim}} > X_{\omega\text{-lim}}$ is confirmed by the present calculation.

Here, we perform the fitting of experimental data. To reduce the number of fitting parameters, we put $\chi_{x^2-y^2} \approx 2\Phi$ by assuming $(U-5J)\sim 0$, which would be justified since the relation $J/U \sim 0.15$ is predicted by the first principle study [41]. Also, we put $\Phi \approx X$ by assuming that $X \gg \chi^{(0)}$. Then, Eqs. (3) and (4) are simplified as

$$C^{-1}_{66} \propto 1/(1-2gX_{k\text{-lim}}), \tag{9}$$

$$\chi^{\text{Raman}}_{x^2-y^2} \propto X_{\omega\text{-lim}}, \tag{10}$$

where $X_{k\text{-lim}} \equiv a_0 T^a\xi^2$ and $X_{\omega\text{-lim}} \equiv b_0(b-T)T\xi^2$: According to Fig. 2, $a\sim 0.5$ and $b\sim 0.1$ for $T > 0.01$.

First, we fit the data of C^{exp}_{66}, which is normalized by the shear modulus due to phonon anharmonicity (33% Co-doped $BaFe_2As_2$ data) given in Ref. [5]. We put $a=0.5$, and the remaining fitting parameters are $h = 2ga_0 l$ and θ. Figure 3(a) shows the fitting result for $Ba(Fe_{1-x}Co_x)_2As_2$: The "dotted line C_{66}" is the fitting result of C^{exp}_{66} under the constraint $C_{66}=0$ at $T=T_S$. We fix $h=2.16$ for all x, and change θ from 116 to -30 K. The "broken line C'_{66}" is the fitting for $x = 0$–0.09 without the constraint, by using $h=2.67$. Thus, both fitting methods can fit the T and x dependences of C^{exp}_{66} very well by choosing only $\theta(x)$ with a fixed h. Figure 3(b) shows the obtained $\theta(x)$ by C_{66} fitting ($x = 0$–0.043) and by C'_{66} fitting ($x = 0.06$, 0.09), as explained above. The obtained $\theta(x)$ is very close to θ_{NMR} given by the Curie-Weiss fitting of $1/T_1T$ [1], which manifests the importance of the AL-VC. Also, θ_{Raman} is given by the Raman spectroscopy [20].

In Fig. 3(c), we show $X_{k\text{-lim}}$ obtained by the fitting of C^{exp}_{66} for $Ba(Fe_{1-x}Co_x)_2As_2$ at $x=0$ and 0.043, We also show $X_{\omega\text{-lim}} \sim X_{k\text{-lim}}(b-T)T^{1-a}$ according to the numerical result in Fig. 2, by putting $b = 1400$ K. In Fig. 3(c), all

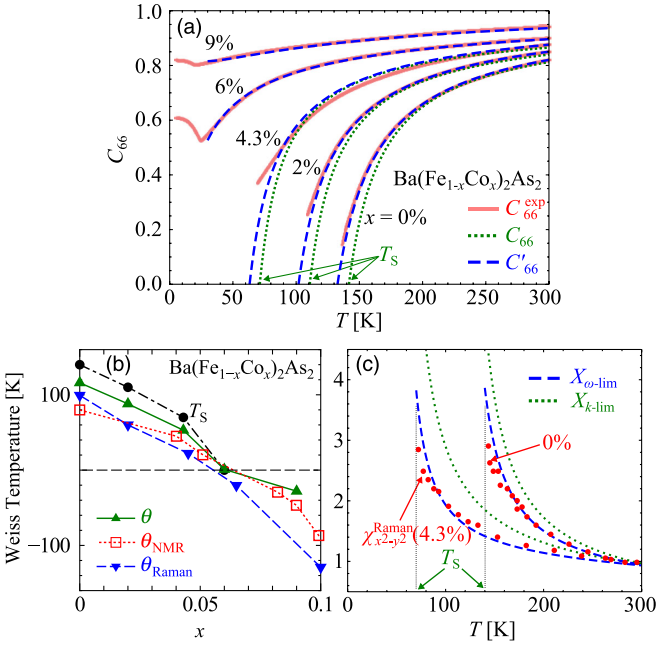

FIG. 3 (color online). (a) Fittings of the data C_{66}^{exp} normalized by the 33% Co-doped $BaFe_2As_2$ data in Ref. [5], shown by broad red lines. The dotted lines C_{66} are the fitting result under the constraint $C_{66} = 0$ at $T = T_S$, and the broken lines C'_{66} are the fitting without constraint. (b) The Weiss temperature θ given by the present fitting. θ_{NMR} is the Weiss temperature of $1/T_1T$ [1], and θ_{Raman} is given by the Raman spectroscopy [20]. (c) $X_{k\text{-lim}}$ and $X_{\omega\text{-lim}}$ given by the fitting of C_{66}. Experimental data of $\chi^{Raman}_{x^2-y^2}$ are shown by red circles [20].

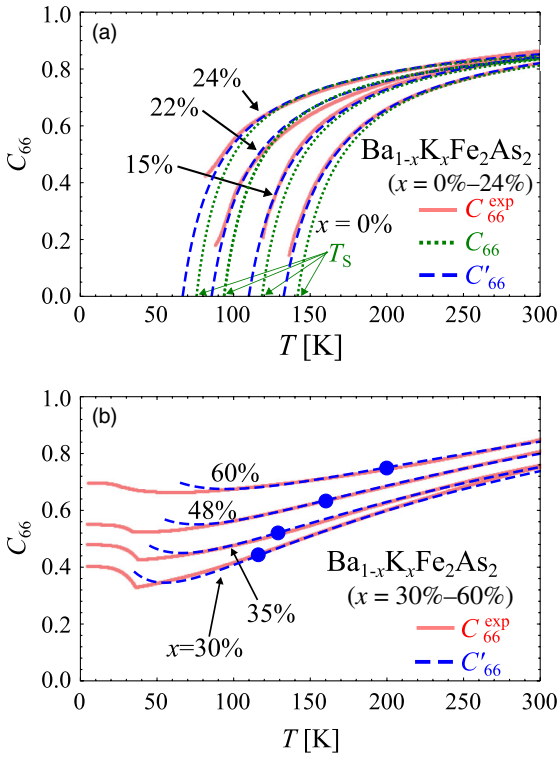

FIG. 4 (color online). Fittings of shear modulus for (a) underdoped and (b) overdoped $(Ba_{1-x}K_x)Fe_2As_2$. Experimental data C_{66}^{exp} are shown by broad red lines [5].

of the data are normalized as unity at 300 K. Then, the relation $\chi^{Raman}_{x^2-y^2} \sim X_{\omega\text{-lim}}$ is well satisfied, as expected from Eq. (10). In addition, the relation $X_{\omega\text{-lim}} \ll X_{k\text{-lim}}$ holds for $T \sim T_S$, consistent with the report in $Ba(Fe_{1-x}Co_x)_2As_2$ [20].

Figures 4(a) and 4(b) show the fitting results for $(Ba_{1-x}K_x)Fe_2As_2$ for $x = 0$–0.24 ($a = 0.5$; $h = 2.16$ for C_{66} and $h = 2.67$ for C'_{66}) and $x = 0.3$–0.6 ($a = 0.58$; $h = 4.98$ for C'_{66}), respectively. In the present theory, we can explain the existence of inflection points of C_{66} in the overdoped region (without structure transition) reported experimentally [5], shown by large blue circles. The inflection point originates from the factor T^a in $X_{k\text{-lim}} \propto T^a\xi^2$. The fitting of overdoped data could be improved by considering the deviation from the relation $X_{k\text{-lim}} \propto T^a\xi^2$ at low T, as recognized in Fig. 2(a). In addition, for $x \gtrsim 0.5$, experimental pseudogap behavior of $1/T_1T(\propto \xi^2)$ below ~100 K [42] would also be related to the inflection point of C_{66}.

In the present theory, we can fit C_{66}^{exp} very well for both overdoped and underdoped regions in $Ba_{1-x}K_xFe_2As_2$. However, a different set of parameters should be used in each region: This fact indicates that the orthorhombic phase and superconducting phase are separated by the first-order transition. In fact, the T^2-like resistivity at the optimum doping $x \sim 0.3$ indicates the absence of the nematic orbital QCP in this compound. We also note that the change in the topology of the electron pockets, called the Lifshitz transition, occurs in $Ba_{1-x}K_xFe_2As_2$ near the optimal doping.

In this Letter, we showed that Raman susceptibility at $\omega = 0$ is enlarged by the AL-VC. The present theory predicts that the ω dependence of the ac Raman susceptibility follows $\chi^{Raman}_{x^2-y^2}(\omega) \sim X(\mathbf{0}, \omega) \sim (1 - i\omega/\Gamma)^{-1}$, and Γ is approximately $\sim\omega_{sf}$. However, Γ could be modified by the ω dependence of $|\Lambda_q(k)|^2$.

In summary, we presented a unified explanation for the softening of C_{66} and enhancement of $\chi^{Raman}_{x^2-y^2}$ based on the five-orbital model. Both $1/C_{66}$ and $\chi^{Raman}_{x^2-y^2}$ are enhanced by the nematic-type orbital fluctuations induced by the AL-VC. However, $\chi^{Raman}_{x^2-y^2}$ remains finite even at the structure transition temperature T_S, because of the absence of the band JT effect and the Pauli (intraband) contribution. The present study clarified that the origin of the nematicity, which is a central issue in Fe-based superconductors, is the nematic orbital order and fluctuations.

We are grateful to A. E. Böhmer for offering us her experimental data published in Ref. [5]. We also thank Y. Gallais, A. V. Chubukov, J. Schmalian, R. Fernandes, and S. Onari for useful discussions. This study has been supported by Grants-in-Aid for Scientific Research from MEXT of Japan.

[1] F. L. Ning, K. Ahilan, T. Imai, A. S. Sefat, M. A. McGuire, B. C. Sales, D. Mandrus, P. Cheng, B. Shen, and H.-H Wen, Phys. Rev. Lett. **104**, 037001 (2010).

[2] R. M. Fernandes, L. H. VanBebber, S. Bhattacharya, P. Chandra, V. Keppens, D. Mandrus, M. A. McGuire, B. C. Sales, A. S. Sefat, and J. Schmalian, Phys. Rev. Lett. **105**, 157003 (2010).

[3] M. Yoshizawa, D. Kimura, T. Chiba, S. Simayi, Y. Nakanishi, K. Kihou, C.-H. Lee, A. Iyo, H. Eisaki, M. Nakajima, and S. Uchida, J. Phys. Soc. Jpn. **81**, 024604 (2012).

[4] S. Simayi, K. Sakano, H. Takezawa, M. Nakamura, Y. Nakanishi, K. Kihou, M. Nakajima, C.-H. Lee, A. Iyo, H. Eisaki, S. Uchida, and M. Yoshizawa, J. Phys. Soc. Jpn. **82**, 114604 (2013).

[5] A. E. Böhmer, P. Burger, F. Hardy, T. Wolf, P. Schweiss, R. Fromknecht, M. Reinecker, W. Schranz, and C. Meingast, Phys. Rev. Lett. **112**, 047001 (2014).

[6] T. Goto, R. Kurihara, K. Araki, K. Mitsumoto, M. Akatsu, Y. Nemoto, S. Tatematsu, and M. Sato, J. Phys. Soc. Jpn. **80**, 073702 (2011).

[7] H.-H. Kuo, J. G. Analytis, J.-H. Chu, R. M. Fernandes, J. Schmalian, and I. R. Fisher, Phys. Rev. B **86**, 134507 (2012).

[8] M. Yoshizawa (private communication).

[9] R. Zhou, Z. Li, J. Yang, D. L. Sun, C. T. Lin, and G. Zheng, Nat. Commun. **4**, 2265 (2013).

[10] F. Krüger, S. Kumar, J. Zaanen, and J. van den Brink, Phys. Rev. B **79**, 054504 (2009).

[11] W. Lv, J. Wu, and P. Phillips, Phys. Rev. B **80**, 224506 (2009); W. Lv, F. Krüger, and P. Phillips, Phys. Rev. B **82**, 045125 (2010).

[12] C.-C. Lee, W.-G. Yin, and W. Ku, Phys. Rev. Lett. **103**, 267001 (2009).

[13] S. Onari and H. Kontani, Phys. Rev. Lett. **109**, 137001 (2012).

[14] H. Kontani, Y. Inoue, T. Saito, Y. Yamakawa, and S. Onari, Solid State Commun. **152**, 718 (2012).

[15] R. M. Fernandes and A. J. Millis, Phys. Rev. Lett. **111**, 127001 (2013).

[16] Y. Ohno, M. Tsuchiizu, S. Onari, and H. Kontani, J. Phys. Soc. Jpn. **82**, 013707 (2013).

[17] M. Tsuchiizu, Y. Ohno, S. Onari, and H. Kontani, Phys. Rev. Lett. **111**, 057003 (2013).

[18] M. Yi, D. H. Lu, J.-H. Chu, J. G. Analytis, A. P. Sorini, A. F. Kemper, B. Moritz, S.-K. Mo, R. G. Moore, M. Hashimoto, W.-S. Lee, Z. Hussain, T. P. Devereaux, I. R. Fisher, and Z.-X. Shen, Proc. Natl. Acad. Sci. U.S.A. **108**, 6878 (2011).

[19] H. Miao, L.-M. Wang, P. Richard, S.-F. Wu, J. Ma, T. Qian, L.-Y. Xing, X.-C. Wang, C.-Q. Jin, C.-P. Chou, Z. Wang, W. Ku, and H. Ding, Phys. Rev. B **89**, 220503(R) (2014).

[20] Y. Gallais, R. M. Fernandes, I. Paul, L. Chauviere, Y.-X. Yang, M.-A. Measson, M. Cazayous, A. Sacuto, D. Colson, and A. Forget, Phys. Rev. Lett. **111**, 267001 (2013).

[21] Y.-X. Yang, Y. Gallais, R. M Fernandes, I. Paul, L. Chauviere, M.-A. Measson, M. Cazayous, A. Sacuto, D. Colson, and A. Forget, arXiv:1310.0934.

[22] K. Kuroki, S. Onari, R. Arita, H. Usui, Y. Tanaka, H. Kontani, and H. Aoki, Phys. Rev. Lett. **101**, 087004 (2008).

[23] P. J. Hirschfeld, M. M. Korshunov, and I. I. Mazin, Rep. Prog. Phys. **74**, 124508 (2011).

[24] A. V. Chubukov, D. V. Efremov, and I. Eremin, Phys. Rev. B **78**, 134512 (2008).

[25] H. Kontani and S. Onari, Phys. Rev. Lett. **104**, 157001 (2010).

[26] S. Onari, Y. Yamakawa, and H. Kontani, Phys. Rev. Lett. **112**, 187001 (2014).

[27] T. Saito, S. Onari, and H. Kontani, Phys. Rev. B **88**, 045115 (2013).

[28] S. Onari and H. Kontani, Phys. Rev. Lett. **103**, 177001 (2009).

[29] Y. Yamakawa, S. Onari, and H. Kontani, Phys. Rev. B **87** 195121 (2013).

[30] S. Onari, H. Kontani, and M. Sato, Phys. Rev. B **81**, 060504 (R) (2010).

[31] S. Onari and H. Kontani, Phys. Rev. B **84**, 144518 (2011).

[32] S. Kasahara, H. J. Shi, K. Hashimoto, S. Tonegawa, Y. Mizukami, T. Shibauchi, K. Sugimoto, T. Fukuda, T. Terashima, A. H. Nevidomskyy, and Y. Matsuda, Nature (London) **486**, 382 (2012).

[33] Y. K. Kim, W. S. Jung, G. R. Han, K.-Y. Choi, C.-C. Chen, T. P. Devereaux, A. Chainani, J. Miyawaki, Y. Takata, Y. Tanaka, M. Oura, S. Shin, A. P. Singh, H. G. Lee, J.-Y. Kim, and C. Kim, Phys. Rev. Lett. **111**, 217001 (2013).

[34] H. Kontani, T. Saito, and S. Onari, Phys. Rev. B **84**, 024528 (2011).

[35] P. Nozieres, *Theory of Interacting Fermi Systems* (Benjamin, New York, 1964); A. A. Abrikosov, L. P. Gorkov, and I. E. Dzyaloshinski, *Methods of Quantum Field Theory in Statistical Physics* (Dover, New York, 1975); A. J. Leggett, Phys. Rev. **140**, A1869 (1965).

[36] H. Kontani and K. Yamada, J. Phys. Soc. Jpn. **65**, 172 (1996); **66**, 2232 (1997).

[37] See Supplemental Material at http://link.aps.org/supplemental/10.1103/PhysRevLett.113.047001 for detailed discussion of the influence of the finite quasiparticle lifetime due to the impurity scattering.

[38] A.-J. Millis, H. Monien, and D. Pines, Phys. Rev. B **42**, 167 (1990); P. Monthoux and D. Pines, Phys. Rev. B **47**, 6069 (1993).

[39] P. Steffens, C. H. Lee, N. Qureshi, K. Kihou, A. Iyo, H. Eisaki, and M. Braden, Phys. Rev. Lett. **110**, 137001 (2013).

[40] The analytic expression of $\Lambda_q^{\omega\text{-lim}}$ is given as

$$\Lambda_q^{\omega\text{-lim}} = \sum_{\alpha,\beta,\gamma}^{\alpha\neq\beta} \sum_{k} \left\{ \frac{1}{\epsilon_k^\beta - \epsilon_k^\alpha} \left(\frac{f_k^\beta}{\epsilon_k^\beta - \epsilon_{k-q}^\gamma} - \frac{f_k^\alpha}{\epsilon_k^\alpha - \epsilon_{k-q}^\gamma} \right) + \frac{f_{k-q}^\gamma}{(\epsilon_{k-q}^\gamma - \epsilon_k^\alpha)(\epsilon_{k-q}^\gamma - \epsilon_k^\beta)} \right\} z_k^\alpha z_k^\beta z_{k-q}^\gamma + \sum_{\alpha,\gamma} \sum_{k} \frac{f_{k-q}^\gamma - f_k^\alpha}{(\epsilon_k^\alpha - \epsilon_{k-q}^\gamma)^2} \{z_k^\alpha\}^2 z_{k-q}^\gamma .$$

[41] T. Miyake, K. Nakamura, R. Arita, and M. Imada, J. Phys. Soc. Jpn. **79**, 044705 (2010).

[42] M. Hirano, Y. Yamada, T. Saito, R. Nagashima, T. Konishi, T. Toriyama, Y. Ohta, H. Fukazawa, Y. Kohori, Y. Furukawa, K. Kihou, C.-H. Lee, A. Iyo, and H. Eisaki, J. Phys. Soc. Jpn. **81**, 054704 (2012).